Phase transformation and microstructural control of the α-solidifying γ-Ti-45Al-2Nb-0.7Cr-0.3Si intermetallic alloy

M. N. Mathabathe[a,b*], S. Govender[a], A. S. Bolokang[a**], R.J. Mostert[b], and C.W. Siyasiya[b]

[a] Counsil of Scientific Industrial Research, Materials Science and Manufacturing, Light Metals, Meiring Naude Road, P O Box 395 Pretoria, South Africa

[b]Department of Material Science and Metallurgical Engineering, Faculty of Engineering, Built Environment and Information Technology, University of Pretoria, South Africa

Abstract

The γ-Ti-45Al-2Nb-0.7Cr-0.3Si based intermetallic alloy was developed. Microstructure evolution of the as-cast and heat-treated alloy yielded the spheriodised and Widmanstätten laths. High temperature differential thermal analysis (HTDTA) was performed on the as-cast Ti-45Al-2Nb-0.7Cr-0.3Si alloy in order to determine critical temperatures and provide insight into phase transformations prior heat treatment. The morphology of the alloy was analysed by the optical microscopy, scanning and transmission electron microscopy (SEM/TEM). The SEM was equipped with energy dispersion spectroscopy (EDS) for chemical composition. The EBSD mapping was employed to determine microstructural evolution. The results show that after heat-treatment the homogeneous microstructures were obtained, compared to the dendritic as-cast structure. The spheriodised laths were seen embedded inside the lamellar structure; whereas the Widmanstätten laths were observed as crossed/needle like (α_2+γ) laths of small spacing, with a spatial orientation with respect to the lamellar structure. The structural development was determined by the X-ray diffraction (XRD).

Keywords: γ-TiAl based alloy, Phase transformation**,** DTA, Heat-treatment, solidification

[*]Corresponding Author: Ms. Maria Mathabathe, Tel: (+27) 12 841 7224

Email: nmathabathe@csir.co.za

[**]Corresponding Author: Dr. Amogelang Bolokang, Tel: (+27) 12 841 3295,

Email: sbolokang@csir.co.za

Graphical Abstract

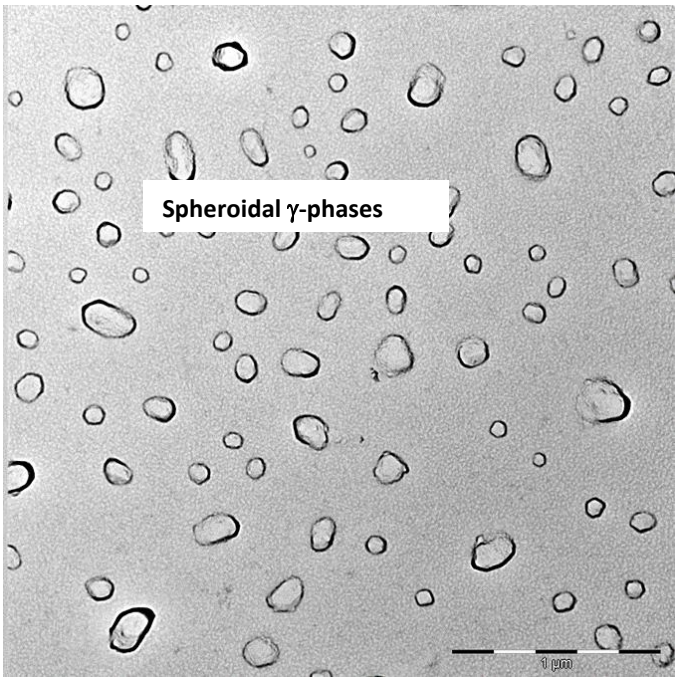

Research Highlights

- Ti-48Al-2Nb-0.7Cr-0.3Si alloy was designed and casted.
- Nb and Cr has stabilised the β-phase in the Ti-48Al-2Nb-0.7Cr-0.3Si alloy.
- Spheriodised phases was induced by the heat treatment process.
- Widmanstätten laths was developed by heat treatment process.
- Phase transformation was realized in the heat treated alloy.

1. Introduction

The γ-TiAl based alloys are materials of particular interest for the production of rotating parts in gas turbine aero engines and for automotive engine application such as engine valves and turbine wheels of turbochargers **[1]**. The main applications and material description for titanium aluminides are well described **[2]**. These intermetallic alloys offer good combination of mechanical properties versus low density, high specific modulus and strength, good creep and oxidation resistance. On the contrary, their limited use to date is property balance, cost and production quality. According to Beddoes et al **[3]**, various microstructures such as mixture of α2 (ordered hcp) + γ-TiAl (ordered fct), duplex microstructure favours tensile properties, whereas the fully lamellar structure enhances fracture toughness and creep resistance as shown in **Fig. 1**.

The melting of titanium alloys is a technologically challenging technique **[4]**. Due to high reactivity of γ-TiAl based alloys, the melting technique should exclude oxygen uptake or partial dissolution of the crucible material. Therefore, vacuum arc re-melting process is widely employed to melt titanium alloys. To establish homogeneity throughout the structure, three melting cycles are sometimes employed. In addition, alloy microstructure could also be controlled by heat-treatment. Depending on the chemical composition and heat-treatment process; γ-TiAl based alloys display four different types of microstructures: near-gamma, duplex, near lamellar and fully lamellar **[5]**. The fully and near lamellar structures consist of TiAl (γ-phase) and a small volume fraction of Ti_3Al (α_2-phase) exhibits good creep and crack-propagation resistance, along with higher fracture toughness. Additionally, higher tensile strength, ductility and longer fatigue life are achieved for an alloy with a duplex structure. Moreover, the microstructure of Ti40Al-10Nb alloys studied showed that the structure of Widmanstätten laths is more creep resistant than the lamellar structure owing to its short mean free path of dislocation slip **[6]**. The mechanical properties of this class of alloys are depended on the microstructure. Various studies have shown that improved tensile strength and ductility for γ-TiAl based alloys can be obtained by

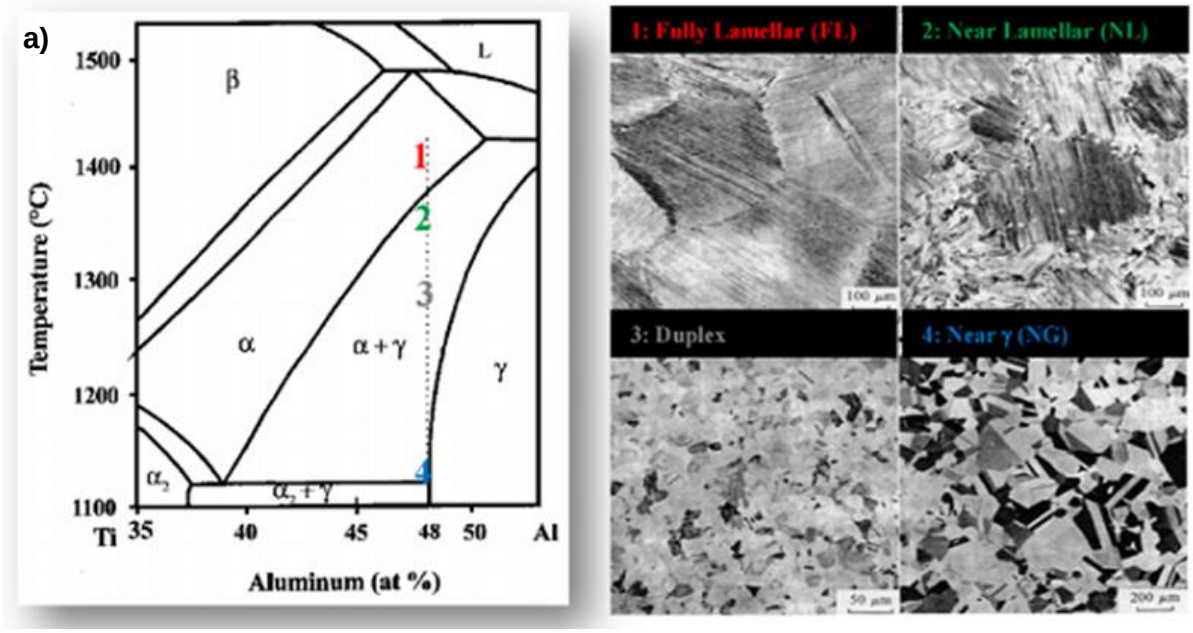

Fig. 1: TiAl phase diagram with corresponding various microstructures **[3]**

grain refinement. Consequently, grain size plays an important role in as-cast γ-based alloys considering that the microstructure often consists of coarse grains commenced from α solidification **[7]**. Clements et al **[8]** reported that solidification path via β-phase is complimentary to obtaining a fine-grained casting microstructure without significant texture and segregation. Additions of Nb, Mo, Cr, W, Ta and V alloying elements enlarge and stabilises the β-phase domain with a bcc crystal structure **[9]**. In the work done by Rajararn **[10]**, the annealed Ti-46.6Al-2.3V-0.9Cr alloy yielded the α plates spheriodised by continuous and discontinuous coarsening, resulting in near-γ structure, which is affected by alloy composition and the morphology of the starting as-cast microstructure. The heat-treatment processes at slightly below Tα can reduce the amount of γ grains drastically, and limit the lamellar grain size in the near-fully lamellar structure, provided the time is short and air cooling is used. Increasing heat treatment time, does not eliminate the untransformed γ grains, which therefore tend to spheriodisation. Furthermore, it is interesting to note that the spheriodised γ laths are located, not only at the lamellar grain boundaries but also within the lamellar grains, which shows that the γ grains do not always impede α grain growth during long time heat-treatment. The kinetics of globularisation of Ti-45.5Al-2Cr-2Nb alloy showed that spheriodisation initiated and proceeded inward from prior α grain boundaries **[11]**. Our current study involves the development of the Ti-45Al-2Nb-0.7Cr-0.3Si and microstructural evolution during the two-step heat-treatment process comprising of solution treating at α phase region, and solidifying into α_2 + γ stable phases at room temperature. The aim of the heat treatment was to induce both the spheriodised and Widmanstätten laths in the Ti-45Al-2Nb-0.7Cr-0.3Si alloy.

2. Experimental procedure

2.1. Raw Materials

The alloy used in this research study (Table 1) was synthesised by small arc button melting furnace under argon atmosphere from pure Ti, Al, Nb, Cr, and Si metallic powders which were blended into the desired composition with subsequent uniaxial pressing in a 43 mm cylindrical dies. The molten green compacts were allowed to cool directly from the copper hearth which is fitted with water cooling jacket in order to aid the solidification process (See Table 2).

Table 1: Chemical composition (at. %) of the alloy

	Ti	Al	Nb	Cr	Si
γ-TiAl alloy	52	45	2	0.7	0.3

Table 2: Heat-treatment parameters

Microstructure	Isothermal treatment	Cooling route
Spheroidised laths	1335 ^{0}C/ for 1h/ ramp to 1350/30mins 10^{0}C/min	Water quench
Widmanstätten laths	1335 ^{0}C/ for 1h/ ramp to down to 1230/30mins at 10^{0}C/min	Air cooling from 1230 ^{0}C

2.2. Thermal analysis

High temperature differential thermal analysis (HTDTA) was performed on the solidified alloy ingot button in order to determine critical temperatures and provide insight into phase transformations. The DTA was conducted using a Shimadzu (DTA-50) instrument, on 3×3×3 mm size specimens cut by electro-discharge machining (EDM). Test specimens, were contained in high purity recrystallized alumina crucible. The DTA cell was continuously evacuated and back-filled with ultra-high purity argon during the heating runs, which were all performed at a heating rate of 20 $^{\circ}$C starting from room temperature to 1500 $^{\circ}$C which was then furnace cooled.

2.3. Heat-treatment process

The heat treatment process was performed in tube furnace flushed with argon gas. The temperature profile for each microstructure is tabulated below:

2.4. Alloy characterization

Metallographic examinations was conducted on as-cast, as-DTA, and as-heat treated specimens, which, were ground up-to 4000 SiC grit papers into a mirror like surface, with subsequent polishing in colloidal silica. In order to reveal the microstructure, Kroll's reagent and electro-polishing were employed. The electrolytic solution used was 600ml methanol, 360ml tert butanol and 60ml perchloric acid The microstructure and the morphology of the phase structures was observed by the scanning and transmission electron microscopy (SEM/TEM) which is equipped with energy dispersion spectroscopy (EDS) for micro-analyses. Reaction products formed during heat treatment process was examined by the X-ray diffraction (XRD). EBSD mapping was also employed to determine microstructure evolution in the heat-treated alloy. Replica technique was used to study surface topography of an etched alloy specimen, in order to be examined in the transmission electron microscope. The technique involved carbon deposition on the specimen surface from an arc source in a vacuum chamber. A dilute solution of (~2%) of Formvar in chloroform is

allowed to run over the surface and then to dry, in order to allow carbon film extraction on small carbon plates.

3. Results and discussion

The microstructure **(Fig. 2)** illustrate the optical micrograph of the as-cast Ti-45Al-2Nb-0.7Cr-0.3Si alloy solidified completely with β-phase as the primary solidification phase. **Fig.2** is a representation of the coarse structure confirmed in the inset image. The inhomogeneity in the structure is shown by the fine and coarse grains with irregular lamellar along with cellular like dendritic structure formed after the melting technique. This behaviour is attributed to the micro-segregation of Nb and Cr to dendrite cores that occurred during solidification process with the resultant remnant primary β-phases after cooling to room temperature. The Nb and Cr are the β-phase stabilisers. The resultant columnar grains has a mixture of lamellar boundaries aligned parallel at 45^{0} angle to the solidification growth direction **[12]**. Furthermore, Ding et al **[13]** reported that β-phase is the primary solidification phase provided that the secondary dendritic arms are orthogonal to the primary arms. During the primary β solidification, it implies that Ti, Nb, and Cr are segregated into the dendrites, whereas the Al is rejected into the inter-dendritic zone.

Fig.3 illustrates the electro-polished SEM/BSE images of the as-cast Ti-45Al-2Nb-0.7Cr-0.3Si alloy. The BSE/SEM examination is a well-known method to validate the existence of different phases in γ-TiAl based alloys [**7]**. The induced phases with different average atomic numbers in composition are highlighted in-terms of different contrast in BSE-mode. **Fig. 3a** shows the conventionally etched SEM micrograph displaying microstructure with β solidification phase verified by the four fold

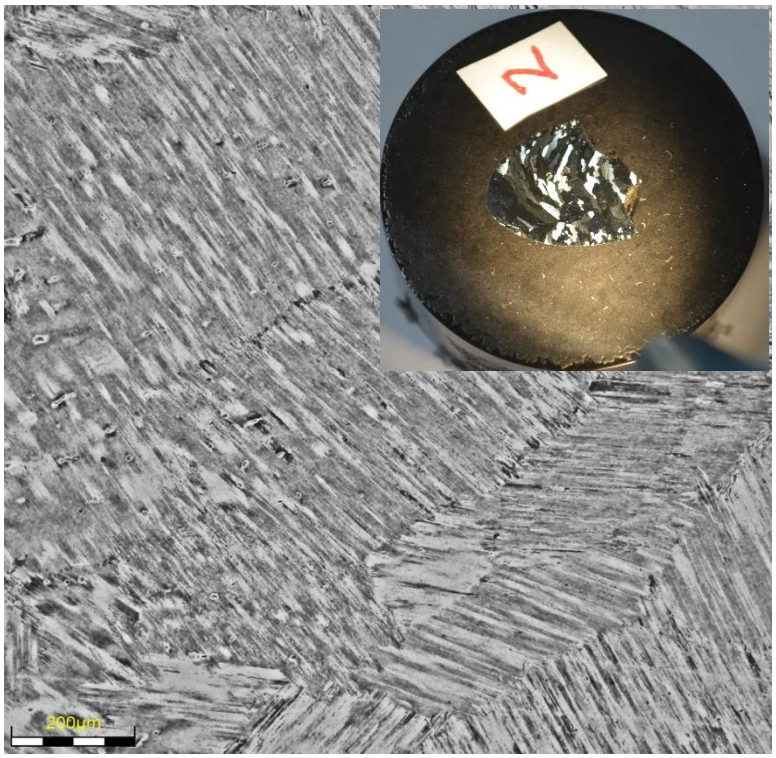

Fig. 2: Optical micrograph of as-cast Ti-45Al-2Nb-0.7Cr-0.3Si alloy and the as-polished sample (inset)

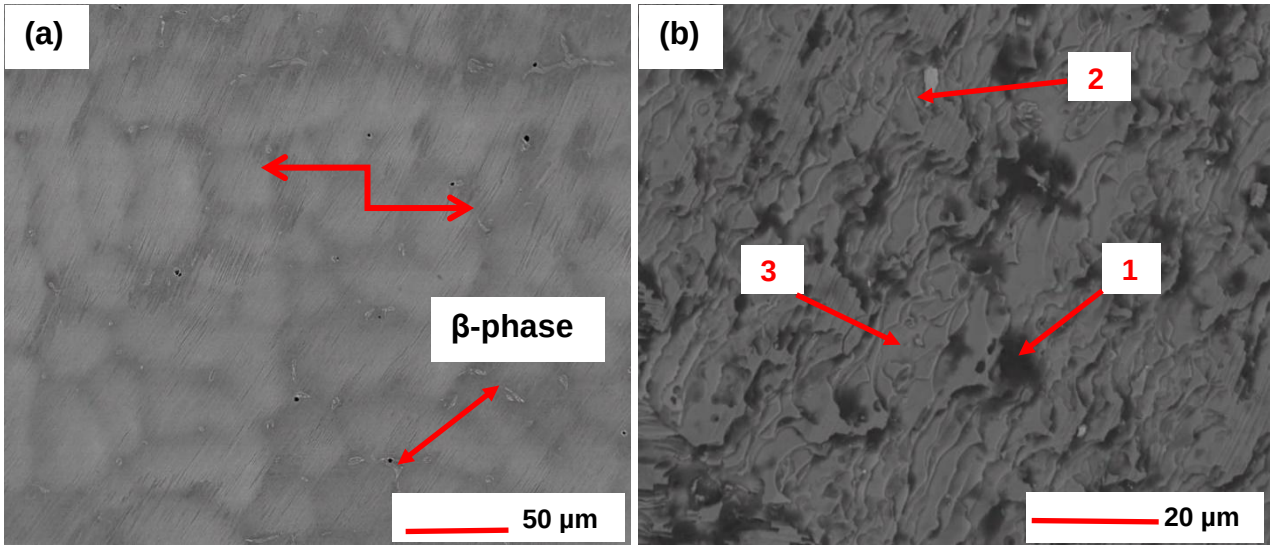

Fig. 3: SEM/BSE micrographs of the as-cast Ti-45Al-2Nb-0.7Cr-0.3Si alloy

Table 3: EDS analysis results of the as-cast Ti-45Al-2Nb-0.7Cr-0.3Si alloy (at.%)

Element	Composition (P1) Fig. 3b	Composition (P2)	Composition (P3)	Matrix Fig. 3b	B-phase Fig. 3b
Al	48.35	22.83	44.28	45.61	48.85
Ti	48.82	54.23	52.24	54.39	46.34
Nb	1.62	1.13	1.53	-	3.04
Cr	0.58	2.00	1.33	-	0.17
Si	0.63	19.81	0.62	-	1.60

symmetry of primary dendrites. Once the peritectic temperature is reached, the α-phase will nucleate and grow from the liquid **[12]**. As the cooling process continues, the solid state transformation will occur with β→α lamellar structure. The consequential final lamellar orientation occurs when the peritectic α-phase consumes the primary β-phase. Zhang et al work **[14]** showed no dendritic core regions implying that the core grains (lamellae) were rich in Al but poor in Cr and Mo, whereas the inter-grain regions phase were rich in Ti, Nb, Cr, respectively. The EDS micro-analysis was conducted in **Fig 3a** following the phases pointed by the arrows while the dark phase confirmed to be rich in Al. The chemical compositions are shown in **Table 3**. The electro-polished SEM/BSE micrograph in **Fig 3b** with the bright phases associated with '**point 2**' showed higher content of in Si, Cr and Nb alloying elements. The white coloured network belongs to the retained primary β-phase due to the presence of Nb and Cr trapping theβ-phase found in pure Ti [**15]**. The EDS analysis presented in '**Point 1**' indicates approximately the equal proportions in atomic composition of Ti indicative of a γ-TiAl phase while **'Point 3'** has Ti content slightly higher than that of the Al in Matrix **(Table 3)**.

In order to establish the phase transformation and determination of heat treatment temperature zones, the as-cast sample was analysed for phase transformation. **Fig.4a** shows DTA curve of the Ti-45Al-2Nb-0.7Cr-0.3Si as-cast alloy. The intermetallic alloy illustrated two sets of melting endothermic peaks within temperature range 900-1431 $^{\circ}$C. The first temperature transition is indicated by the endothermic peak onset at 966 $^{\circ}$C and completed at 1030 $^{\circ}$C, which is thought to be $\alpha_2 + \gamma \rightarrow \alpha$-phase transformation. The second endothermic peak occurred between 1151 $^{\circ}$C and 1431 ^{0}C attributed to $\alpha \rightarrow \alpha + \beta$. However, this transition is seen to be extremely broad compared to the first one; with evidence of more than one reaction from an observation of a sudden change in slope at 1271 $^{\circ}$C, indicating the occurrence of the major solid-state reactions. The metallographic examination of the DTA sample after thermal analysis is shown in **Fig.4b**. The microstructure is inhomogeneous and comprised of fine and coarse grains with irregular lamellar structure. The profoundly seen white network shown by the double black arrow represent the β-phase. It should be noted that the DTA sample attributes mainly the

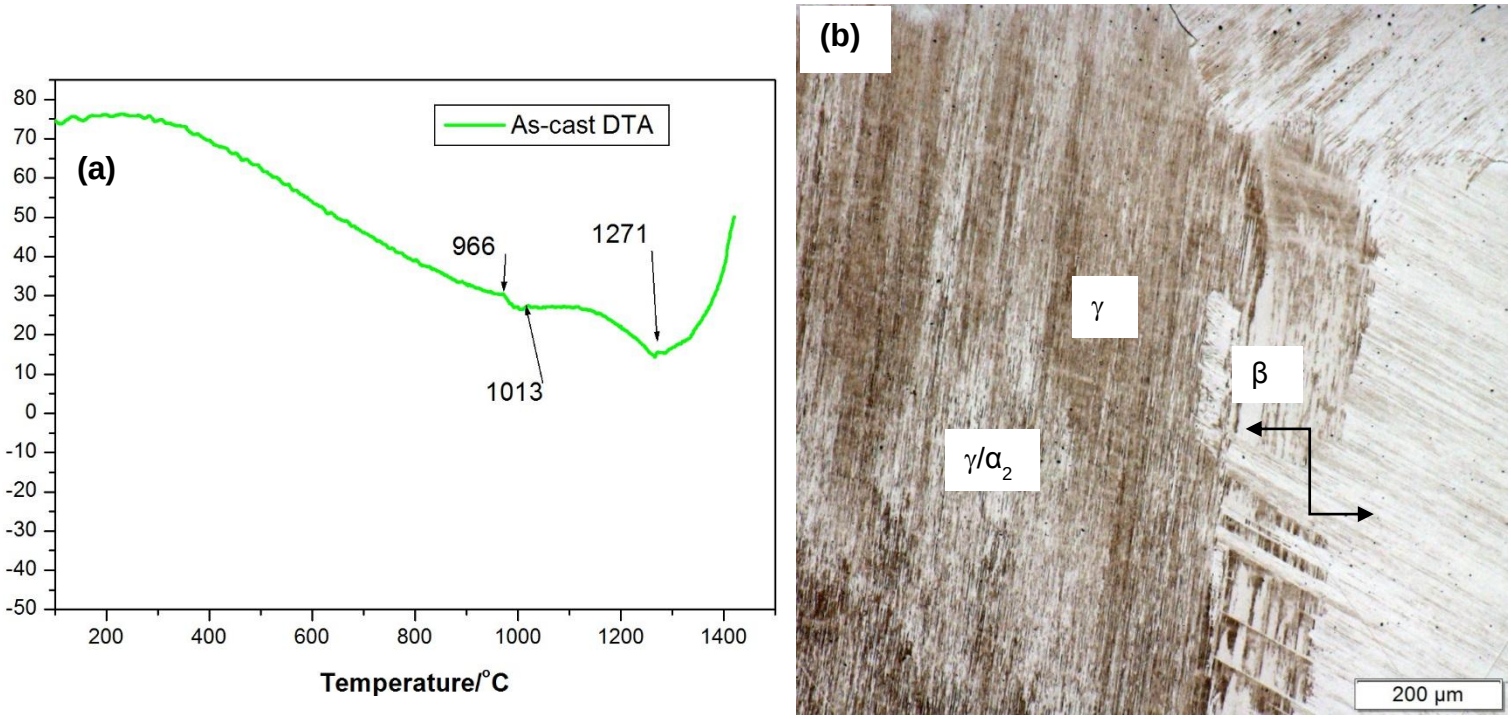

Fig.4: a) DTA of the as-cast Ti-45Al-2Nb-0.7Cr-0.3Si alloy and the (b) optical microstructure of the Ti-45Al-2Nb-0.7Cr-0.3Si sample after thermal analysis

characteristics of the annealing process since the sample cool down slowly with the heating chamber.

Fig.5 shows the SEM/BSE image consisting of Widmastätten laths inside the lamellar structure. The lamellar structure are mainly observed along colony boundaries, and represent sites of increased internal stresses coupled with locally higher dislocation densities **[16]**. Furthermore, the Widmanstätten colonies (needle-like in a random direction) are formed inside lamellar grains with small spacing **[17]**, through twinning or recrystallization, and forms from the α-grains that have different orientation compared to the surrounding material. The driving force for such a structure is the supercooling occurring at the applied cooling rate. The growth mechanism of different structures depended on the cooling rate. These are long straight lamellar packets presenting nearly no disorientation between themselves and are embedded inside the lamellar structure but with different spatial orientation (Widmanstätten laths), monitored under a range of intermediate cooling rate such as air, sand, and oil-quenched **[18]**. The spheriodised sample had lamellar structure (α_2 γ+) with certain areas demonstrating equiaxed γ-phase and Ti_5Si_3 precipitates as shown in supporting file **S1**. It can be noted that the microstructure of the α-solidifying water-quenched alloy exhibit fine and homogeneous microstructure with no evidence of the β-phase compared to the sample after thermal analysis. The phases present in the microstructure were analysed for chemical composition. The EDS chemical composition is presented in **Table 4**. The titanium silicate (Ti_5Si_3) phase was formed due to the presence of Si in the alloy.

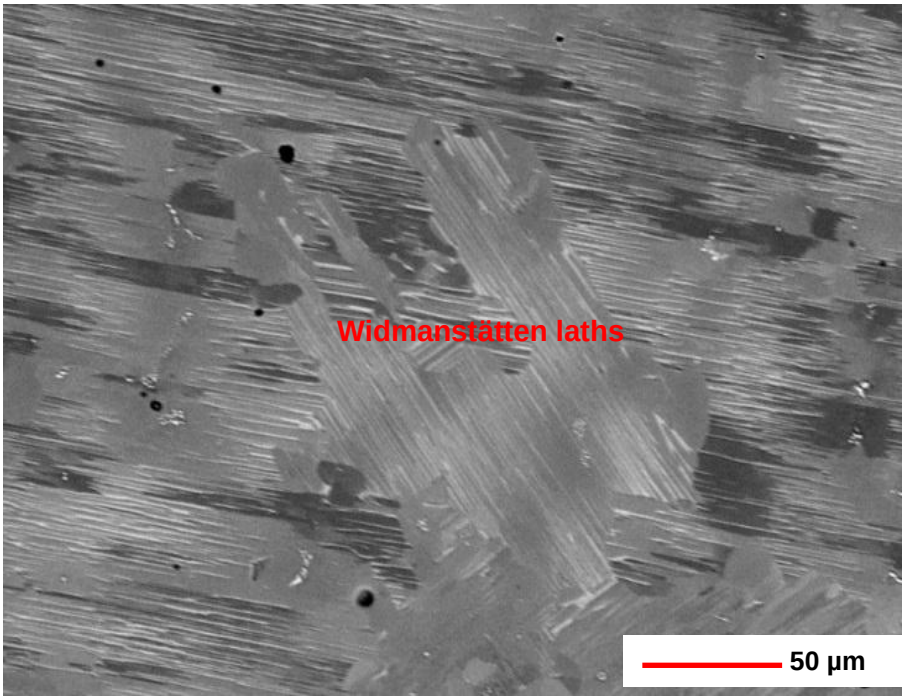

Fig.5: SEM image of the Ti-45Al-2Nb-0.7Cr-0.3Si alloy after (a) spheriodisation and with Widmanstätten laths

Table 4: EDS analysis results of the spheriodised Ti-45Al-2Nb-0.7Cr-0.3Si alloy (at.%)

Element	**Composition (P1) Fig. 3b**	**Composition (P2)**	**Composition (P3)**	**Ti_5Si_3 phase**
Al	48.29	35.60	46.15	18.84
Ti	48.27	60.20	46.88	56.64
Nb	1.68	1.66	1.61	1.45
Cr	0.62	1.31	0.53	0.92
Si	1.13	1.23	4.83	22.16

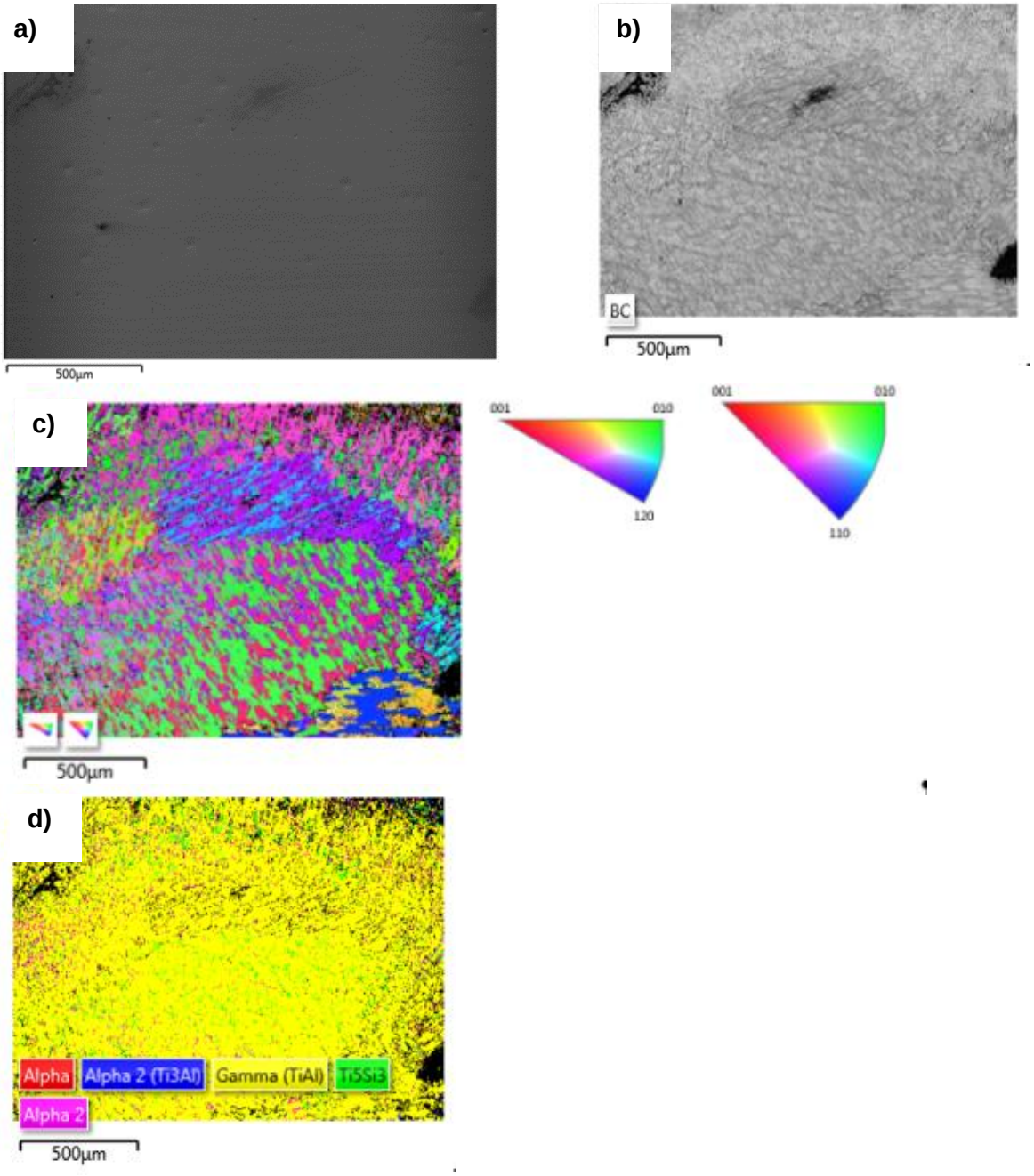

Fig. 6: EBSD maps of the spheriodised Ti-45Al-2Nb-0.7Cr-0.3Si alloy: a) Electron micrograph; b) Band contrast image; c) Inverse pole figure (IPF) maps and d) Phase colour map

Fig.6 shows the EBSD maps of the Ti-45Al-2Nb-0.7Cr-0.3Si spheriodised alloy. It is clear that a large number of γ-grains are recrystallized. However, grain orientation of the recrystallized γ-grains are almost random **(Fig.6c)**, which imply that there is no obvious texture attained during the spheriodising heat-treatment. **Fig.6d** illustrate the phase colour map, with dominating γ-TiAl phase. Furthermore, **Fig.6c** show the obtained orientation map with a tetragonal structure (*c/a* = 1.45), respectively. Zambaldi **[4]** pointed out that correct detection of order domain structure is given by the distribution of pattern quality. The position of order domain boundaries is shown by the reduced sharpness of the Kikuchi bands, which may result from misfit stresses and defects along the boundaries, and therefore lower values in the pattern quality maps **[4]**. In **Fig.6c** the identified domain boundaries follow the lines of the band contrast **Fig.7b**. The band contrast image in **(Fig.6b)** display small spheriodised γ-phases between the lamellae structures. Moreover, the TEM micrograph in **Fig. 7a-b** is the confirmation of the spheriodised and long Widmanstätten colonies of needle-like laths in a random direction.

The X-ray diffraction pattern in **Fig.8** confirm the phases present in the microstructures. The Ti-45Al-2Nb-0.7Cr-0.3Si alloys exhibited ordered γ-TiAl with a tetragonal lattice structure and ordered α_2-Ti_3Al with a close-packed hexagonal lattice. Concurrently, few peaks of retained β-phases and Ti_5Si_3 were detected. The β-phases, are only seen on the as-cast and on the thermally analysed DTA sample. The spheriodised sample as well as the sample with Widmanstätten laths showed new XRD peaks validating the occurrence of the phase transformation after heat treatment.

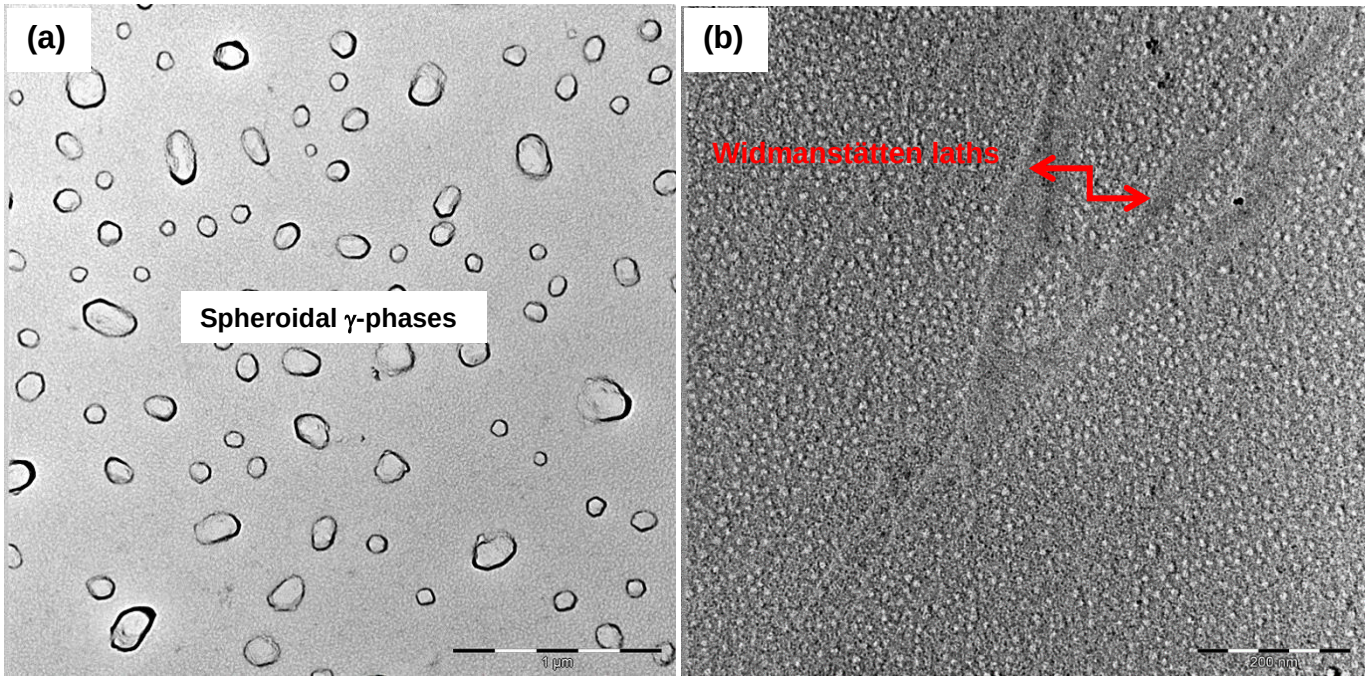

Fig. 7: TEM image of the Ti-45Al-2Nb-0.7Cr-0.3Si alloy indicative of (a) spheriodised and (b) Widmanstätten laths

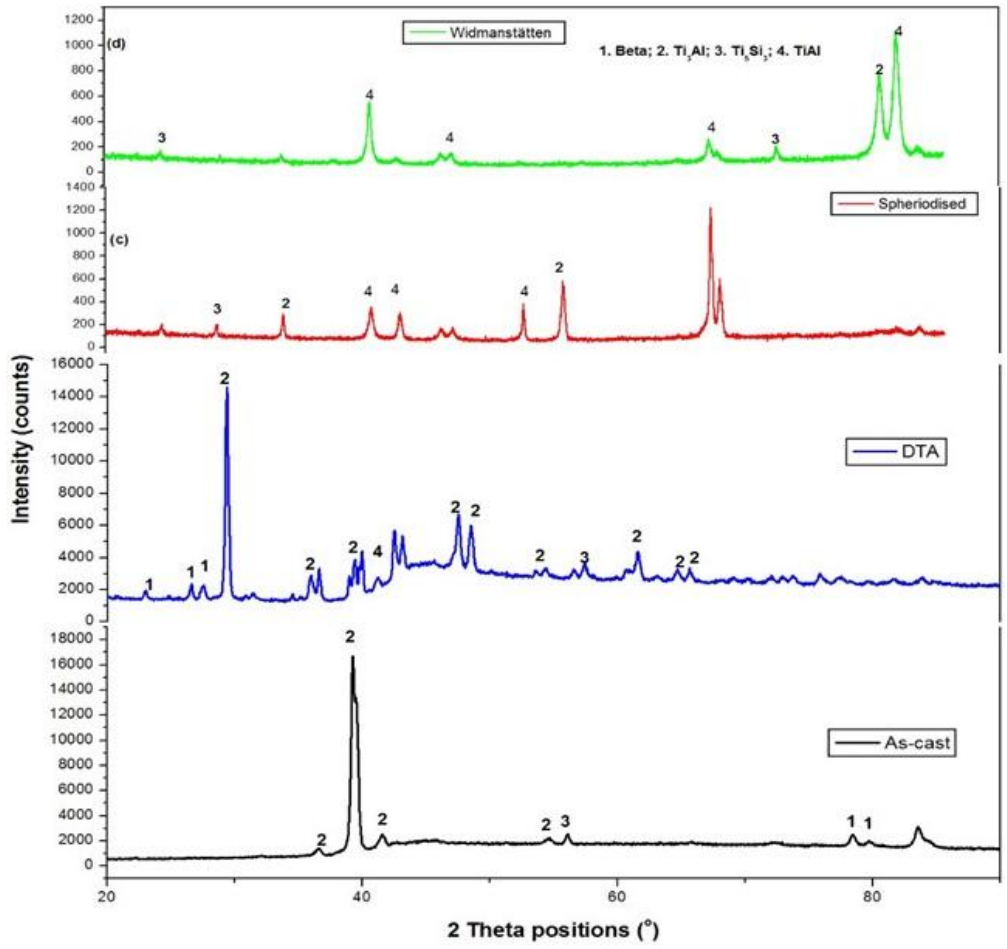

Fig. 8: XRD pattern of the (a) as-cast, thermally analysed (c) spheriodised and (d) Widmanstätten induced Ti-45Al-2Nb-0.7Cr-0.3Si alloy

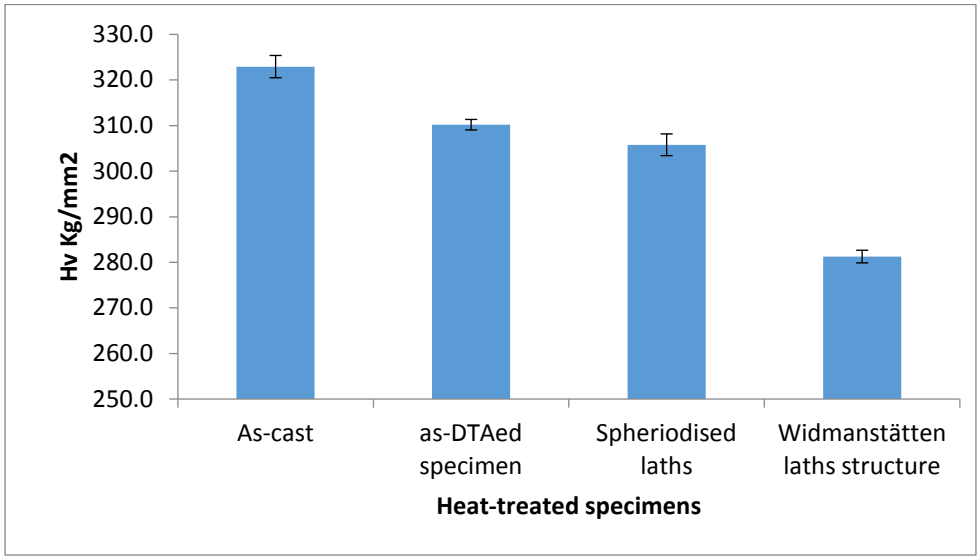

Fig. 9: Macro-hardness of the of the as-cast, thermally analysed, spheriodised and Widmanstätten induced Ti-45Al-2Nb-0.7Cr-0.3Si alloy microstructures

Fig.9 illustrates the macro-hardness of the Ti-45Al-2Nb-0.7Cr-0.3Si alloy in the as-cast, thermally analysed (DTA), spheriodised and as-Widmanstätten laths condition. The hardness properties of the Ti-45Al-2Nb-0.7Cr-0.3Si alloy may have a linear relationship with the yield stress in directionally solidified alloy reflecting the processing performance in yielding mechanical properties to be estimated. The as-cast and the DTA specimens has high hardness values compared to those heat-treated samples. The Widmanstätten lath structure is comprised of the lowest hardness value compared to all samples due to weaker grain boundaries. Due to high density of internal boundaries after the melting process, a hardness of 322.9 HV was measured higher than 281.2 HV. The as-cast sample and the DTA specimen has coarse grained microstructure exhibiting lamellar colonies and γ-grains as well as few retained β-phases; which may be attributed to solidification path induced by the addition of Nb and Cr contents, and fast solidification effect due to the melting method. For the current alloy the β-phase is contemplated inside the lamellar structure and along the boundaries of the colonies indicating that the β-phase is the primary solidification phase. Moreover, the preferential growth of β-phase during solidification is <100> axis. There are three equivalent directions, namely [100], [010], and [001], as a result the alloys demonstrates columnar characteristics much less pronounced to the case of α solidification **[7]** (as indicated by **Fig. 3a** and EBSD mapping in **Fig.6**).

In order to obtain the spheriodised lath structure, the alloy was subjected to solution treatment in the α-phase field, with abrupt holding at the (α+γ) followed by water quenching from 1350 ^{0}C. However, during cooling the α-phase transformed to lamellar structure (α_2 + γ) or γ-phase. The remnant β-phase from the as-cast alloy upon quenching at 1350 ^{0}C decomposed to acicular α-phase via secondary lath formation at high cooling rates **[19]**. Addition of Si in the current Ti-45Al-2Nb-0.7Cr-0.3Si alloy improved room temperature ductility as shown by low hardness values, possible low oxidation resistance and improved creep properties at high temperatures not reported on the current study **[20]**.

As indicated in **Fig. 1a**, TiAl with the composition of about 48 (at %) Al content solidifies with three primary solidification phases and two peritectic reactions as follows **[18]**;

$$L \rightarrow \beta + L \rightarrow \beta + L + \alpha \rightarrow L + \alpha \rightarrow \alpha \rightarrow \alpha + \gamma \rightarrow \alpha_2 + \gamma \quad (1)$$

The γ-TiAl based alloy is heated into the α single phase region, the Al becomes effectively dissolved in the hexagonal closed packed Ti. Furthermore, if the pre-existing microstructure is the γ-phase segregated with α-phase, the dendritic segregation will dissolve and the microstructure will become homogeneous. It was found that the γ-grains dissolves through diffusion controlled dissolution **[18]**, as shown by equation 2:

$$\frac{D_\alpha}{dt} = k^* \left[\left(\frac{1}{D_\alpha}\right) - \left(\frac{1}{D_\alpha^L}\right)\right]^{P-1} \quad (2)$$

Where Dα denotes grain size of the α grain as a function of time, k* denote the rate constant, D_α^L denotes the α-grain size limit, and p denotes the grain growth exponent. The heat-treatment process that produced Widmanstätten laths transformed the coarse grained inhomogeneous microstructure of as-cast Ti-45Al-2Nb-0.7Cr-0.3Si into a homogeneous structure, with refined lamellar spacing. Therefore, extensive TEM analysis will be critical for future investigation of these alloys.

4. Conclusion

The Ti-48Al-2Nb-0.7Cr-0.3Si alloy was designed and casted. In this study microstructure evolution, phase transition and hardness were investigated on the as-cast, DTA and heat treated alloys. The β-segregation in the as-cast and as-DTA conditions were induced by the Nb, and Cr enrichment in the primary β or α-phase during the solidification; and in the retained β-phase during the $\beta \rightarrow \alpha$ transition, in which β-segregation adds greatly in the Nb-enrichment in the final structure. The heat-treated alloy is indicative of the homogeneous α_2/γ lamellar structure discovered during the primary α-phase solidification. The EBSD mapping revealed the microstructure evolution via the heat-treatment in the as-cast alloy, in which spheriodised laths were ascertained in the band contrast map. TEM micrograph

confirmed the spheriodised and Widmanstätten laths embedded inside the lamellae. Whereas, the XRD results approved of the phases present in the microstructure. Phase transformation and microstructural evolution of an α-solidifying Ti-48Al-2Nb-0.7Cr-0.3Si alloy was determined, and as a result a homogeneous microstructure with spheriodised/ Widmanstätten laths along the lamellae were obtained. Widmanstätten laths were observed as long and straight laths embedded inside the lamellar structure that assume a partial orientation.

5. Acknowledgements

Department of Science and Technology (DST) and Council of Scientific Industrial Research (CSIR) is acknowledged for funding this work. Finally, the technical support from the University of Pretoria and Mintek mainly for the provision of some of the laboratory equipment's.

6. References

[1]. G. Baudana, S. Biamino, B. Kloden, A. Kirchner, T. Weißgarber, B. Kieback, M. Pavese, D. Ugues, P. Fino, C. Badini, Electron Beam Melting of Ti-48Al-2Nb-0.7Cr-0.3Si: Feasibility investigation, Intermetallics, 73 (2016) 43–49.

[2] K. Kothari, R. Radhakrishnan, N. M. Wereley, Prog. Aerosp. Sci. Advances in gamma titanium aluminides and their manufacturing techniques, 55 (2012)1–16.

[3] J. Beddoes, W. Wallace, L. Zhao, Int. Mater. Rev. Current understanding of creep behaviour of near γ-titanium aluminides, 40 (5) (1995) 197–217.

[4] C. R. Zambaldi, Micromechanical modeling of γ -TiAl based alloys. 2010.

[5] J. Lapin and M. Nazmy, Microstructure and creep properties of a cast intermetallic Ti-46Al-2W-0.5Si alloy for gas turbine applications, Mater. Sci. Eng. A, 380 (1) (2004) 298–307.

[6] C. J. Zhang, T. H. Yu, and C. H. Koo, Creep behavior of Ti-40Al-10Nb titanium aluminide intermetallic alloy, Mater. Sci. Eng. A, 435–436 (1) (2006) 698–704.

[7] Y. Wang, Y. Liu, G. Y. Yang, H. Z. Li, and B. Tang, Microstructure of cast gamma-TiAl based alloy solidified from beta phase region, Trans. Nonferrous Met. Soc. China. 21 (2) (2011) 215–222.

[8] H. Clemens, A. Bartels, S. Bystrzanowski, H. Chladil, H. Leitner, G. Dehm, R. Gerling, F.P. Schimansky, Grain refinement in γ-TiAl-based alloys by solid state phase transformations, Intermetallics, 14 (12) (2006) 1380–1385.

[9] G. Liu, Z. Wang, T. Fu, Y. Li, H. Liu, T. Li, M. Gong, G. Wang, Study on the microstructure, phase transition and hardness for the TiAl-Nb alloy design during directional solidification, J. Alloys Compd., 650 (2015) 45–52.

[10] S. Rajararn, “A heat tretment procedure to produce fine grained lamellar microstructures in a P/M titanium aluminide alloy,” PhD thesis, 1996.

[11] R. V. Ramanujan, Phase transformations in γ based titanium aluminides, Int. Mater. Rev. 45 (6) (2000) 217–240.

[12] H. Saari, J. Beddoes, D. Y. Seo, and L. Zhao, Development of directionally solidified γ-TiAl structures, Intermetallics, 13 (9) (2005) 937–943.

[13] X. F. Ding, J. P. Lin, L. Q. Zhang, H. L. Wang, G. J. Hao, and G. L. Chen, Microstructure development during directional solidification of Ti-45Al-8Nb alloy, J. Alloys Compd. 506 (1) (2010) 115–119.

[14] D. Zhang, E. Arzt, and H. Clemens, Characterization of controlled microstructures in a gamma-TiAl(Cr, Mo, Si, B) alloy, Intermetallics. 7 (10) (1999) 1081–1087.

[15] A.S. Bolokang, D.E. Motaung, C.J. Arendse, T.F.G. Muller, Formation of the metastable FCC phase by ball milling and annealing of titanium–stearic acid powder, Advanced Powder Technology 26 (2015) 632–639.

[16] W. Schillinger, H. Clemens, G. Dehm, and A. Bartels, Microstructural stability and creep behavior of a lamellar ??-TiAl based alloy with extremely fine lamellar spacing, Intermetallics, 10 (5)(2002) 459–466.

[17] S. F. Franzén and J. Karlsson, γ-Titanium Aluminide Manufactured by Electron, Metal Powder Report. 71 (3) (2016) 193-199.

[18] S. R. Dey, A. Hazotte, and E. Bouzy, Crystallography and phase transformation mechanisms in TiAl-based alloys – A synthesis, Intermetallics, 17 (12((2009)1052–1064.

[19] Y. Jin, J. N. Wang, J. Yang, and Y. Wang, Microstructure refinement of cast TiAl alloys by beta solidification, Scr. Mater 51(2) (2004) 113–117.

[20] F. Sun and F. H. S. Froes, Solidification behaviour of Ti5Si3 whiskers in TiAl alloys, Mater. Sci. Eng. A. 328 (2002) 113–121.